Characteristic Analysis of Power Oscillations Caused by Disharmony Among Voltage-source-controlled Units in Three-terminal Local Power Grid

Qiyi Yu and Yi Tang, *Senior Member*, *IEEE*

***Abstract*—Previous studies have demonstrated that disharmony among voltage-source-controlled units (VSCUs) may occur on an alternating current (AC) transmission or distribution line under steady-state operating conditions (SSOCs) or quasi-static operating conditions (QSSOCs). As the studies on frequency disharmony have been expanded to multiple disharmonized VSCUs in the local power grid, its adverse effects on AC lines and equivalent load (EL) at the bus without active voltage control ability (non-active bus) need to be investigated further. Considering the locality of disharmony and common topological connections among VSCUs, this paper adopts a Y-type three-terminal local power grid (LPG) as the research object. The disharmony among the three VSCUs is discussed. Firstly, for the load at non-active bus, the formulas for single-phase instantaneous voltage, load current, load power, as well as average power under disharmony operating conditions (DOCs) are derived. The characteristic indicators of the above electrical quantities are defined, which can measure the amplification and reduction degrees of the above electrical quantities before and after disharmony. Secondly, for the line directly connected to VSCUs, the formulas for single-phase instantaneous line current and power and the average power under DOCs are derived. The characteristic indicators of power flow are defined, which can be used to quantify the peak amplification impact of oscillation before and after disharmony. Finally, the case study on the Y-type three-terminal LPG under the single-disharmony and the multi-disharmony switching scenarios indicates that the long-period power oscillation caused by disharmony may occur in the load flow at the non-active bus and the line flow. The oscillation causes a serious decrease in load capability and a significant amplification of the peak of line power oscillation.**

***Index Terms*—New power system, power oscillation, disharmony, voltage-source-controlled unit (VSCU), characteristic analysis.**

I. Introduction

THE power grid is constantly subject to large or small disturbances [1] - [3]. Grid-connected synchronization units such as synchronous generator and converter-interfaced units may lose synchronization with other equipment or with the power grid under disturbances [4] - [7]. To solve the impact of synchronization instability on the power grid, the characteristics of the synchronization stability must be thoroughly investigated. Based on the devices involved and control strategy, synchronization instability can be divided into three categories: ① instability of synchronous generator; ② instability of grid-following (GFL) converter; ③ instability of grid-forming (GFM) converter. The instability of the above three categories includes two types [8], i.e., small-signal instability and large-disturbance instability.

For the instability of synchronous generator, the small-signal instability is usually associated with insufficient damping of oscillations, which can result in oscillations of the rotor angles. Large-disturbance instability is usually associated with insufficient synchronizing torque, which can cause aperiodic separation of the rotor angles.

For the instability of GFL converter, the small-signal instability caused by phase-locked loop (PLL) in power grids with low short-circuit ratio (SCR) has been adequately studied in existing literature. Reference [9] reveals that the proportional gain of the current controller essentially aggravates the instability effect of PLL. This instability is more prone to arising with the increase of PLL bandwidth [10] and the decrease of SCR [11]. Large-disturbance instability may occur for two reasons. ① There are no equilibrium points due to high R/L ratio [12], severe faults [13], or excessive output current [14], [15]. ② There is not enough damping to reach an equilibrium point [14]-[16]. Furthermore, the effect of factors such as constant reactive power control [12], PLL frequency limiter [16], and typical control limiters [17] on stability is investigated.

For the instability of GFM converter, the small-signal instability may occur in stiff power grids and series-compensated weak power grids. It is related to the power-frequency dynamics of the inverters, power grid characteristics, and power grid impedances [18] - [20]. Large-disturbance instability may occur for two reasons [21]-[23]: ① an unexpected equilibrium point; ② no equilibrium points due to overcurrent

Manuscript received: August 24, 2023; revised: December 4, 2023; accepted: January 29, 2024. Date of CrossCheck: January 29, 2024. Date of online publication: March 22, 2024.

This work was supported by Science and Technology Project of State Grid Corporation of China "Research on new energy grid-connection control methods and key technologies to improve power grid security and stability" (No. 5100-202140498A-0-5-ZN).

Q. Yu and Y. Tang (corresponding author) are with the School of Electrical Engineering, Southeast University, Nanjing 210018, China (e-mail: yqypaper@126.com; tangyi@seu.edu.cn).

DOI: 10.35833/MPCE.2023.000519

limiter, which prevents the output active power from reaching the reference value. Furthermore, the dynamics of a typical GFM control are characterized in [24]. It is reported that the droop control and the voltage source grid-connected (VSG) control can be destabilized due to the lack of damping on their inertial transient responses. Reference [25] shows that the interaction between voltage outer loop and current inner loop also aggravates the instability under large disturbances.

The above instability problems are mainly concerned with the phase or rotor angle difference caused by non-zero frequency difference between grid-connected synchronization units, or phase difference between these units with the same frequency under small or large disturbances. It is generally assumed that the frequencies of the nodes are the same under steady-state operating conditions (SSOCs) after restoration. Meanwhile, there is a lack of research works on small frequency differences under SSOCs and their effects. Nevertheless, it is worth noting that the unregulated power oscillations with an average period of one hour related to frequency fluctuations as well as long-term oscillations and resonance due to asynchronous operation have been observed in conventional power system of the former Soviet Union [26]. Considering the weak synchronization of new power system, similar oscillations will be developed at the grid level, which will be discussed below in combination with Fig. 1. $\boldsymbol{U}_{\text{sabc}}$ and $\boldsymbol{I}_{\text{sabc}}$ are the three-phase voltage and current of voltage source controlled unit (VSCU), respectively; ω_{sref} and U_{sref} are the reference frequency and voltge, respectively; and θ_f is the output phase angle of GFM control.

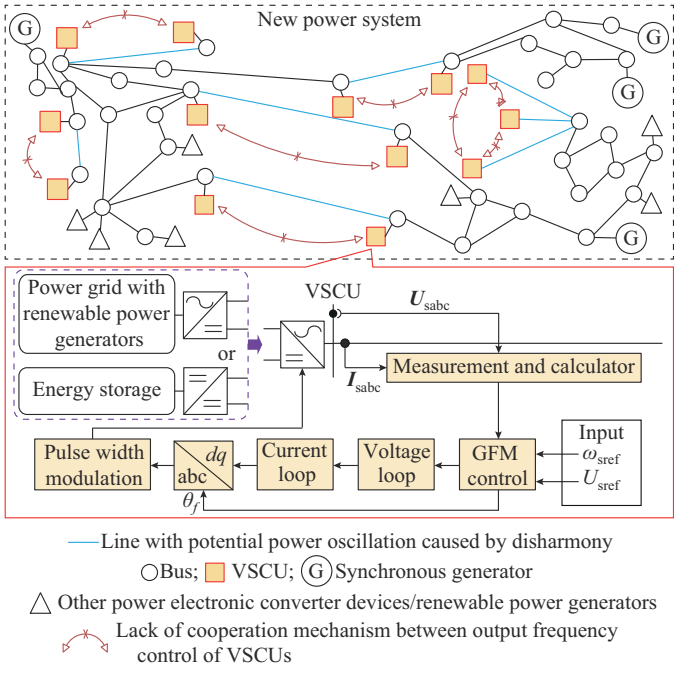

Fig. 1. New power system with disharmonized VSCUs.

First, the inertia is reduced due to high proportion of renewable power generators and power electronic converter devices including some kinds of VSCUs in the new power system. They can impair the foundation of frequency unification in the entire AC power grid, and thereby weaken the phase-synchronization ability of AC power grid under non-fault operating conditions. Second, the proliferation of VSCUs may lead to a sharp decline in frequency-harmonization ability in the local power grid (LPG) due to the output frequency differences among VSCUs. The cooperation mechanism between the output frequency control of VSCUs under distributed synchronous GFM mode is lacking [27]. The lack of cooperation mechanism easily leads to poor harmonization ability of VSCUs in the LPG. As a result of the weak synchronization and harmonization abilities, the disharmony phenomenon may occur on an AC line under SSOCs or quasi-static operating conditions (QSSOCs). Namely, the output frequency of each VSCU at the sending and receiving buses or multiple VSCUs at different buses is not equal for a longer time, and the mean value of frequency difference between any two of them is non-zero. We have previously investigated the power oscillation on AC transmission line caused by disharmonized VSCU at the sending and receiving buses and revealed that the amplification effect of power oscillation peak may threaten the safety of operation [27]. VSCUs are not only installed at both sides of an AC transmission line, but also connected to the LPG. Disharmony among VSCUs is likely to occur owing to the lack of frequency cooperation control. This new type of disharmony phenomenon may affect the power flow on AC lines and load at non-active bus.

This paper analyzes the characteristics of load power oscillation and line power oscillation for a three-terminal network integrated with three disharmonized VSCUs. Compared with our previous research works, the main contributions of this paper are as follows.

1) Based on Y-type three-terminal LPG, the abnormal characteristics of equivalent load (EL) at non-active bus and power flow on AC line directly connected to VSCUs under disharmony operationg conditions (DOCs) are analyzed. The formulas for main electrical quantities of non-active bus and AC line are derived to carry out the power flow calculation under DOCs.

2) The weak load capacity of non-active bus and peak multiplication impact under DOCs is revealed. The effects of initial phase difference and disharmony period on load capacity and multiplication impact are investigated via sensitivity analysis.

3) The grid-side power oscillation under the single-disharmony and the multi-disharmony switching scenarios is analyzed. Oscillation characteristics of average power of EL at non-active bus and line power in real power grids are discussed. Moreover, the negative impacts of power flow fluctuation on the load capability of non-active bus and line power are highlighted.

This paper is organized as follows. Section II elaborates on the equivalent model of three-terminal LPG with disharmonized VSCUs. Section III analyzes abnormal voltage and power characteristics of non-active bus with disharmonized VSCUs. Sections IV and V analyze the characteristics of line current oscillation and line power oscillation with disharmonized VSCUs, respectively. Section VI presents the case study and analysis results, and Section VII concludes this paper.

II. Equivalent Model of Three-Terminal Network with Disharmonized VSCUs

Oscillation caused by disharmony often manifests as a local problem of AC power grid originating from frequency disharmony among nearby VSCUs or between a VSCU and equivalent AC power grids. Typically, the electrical connection between three neighboring VSCUs in the LPG is often a star-type topological structure. The general structure of a Y-type three-terminal LPG with three disharmonized VSCUs connected is given in Fig. 2(a).

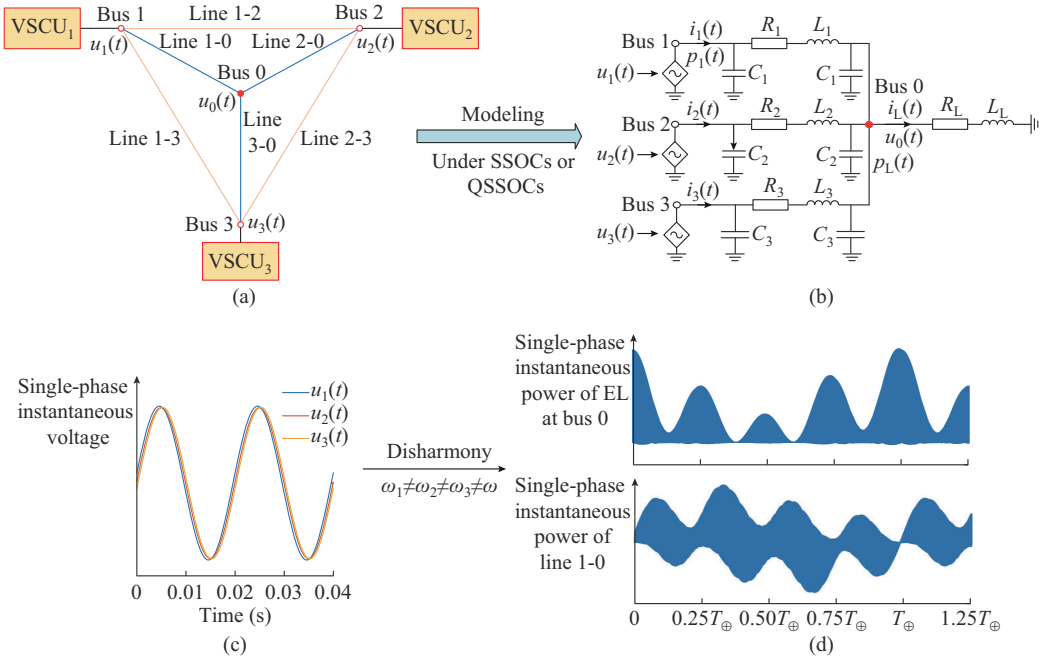

Fig. 2. General structure of a Y-type three-terminal LPG with disharmonized VSCUs and characteristics analysis. (a) General structure of a Y-type three-terminal LPG with three disharmonized VSCUs. (b) Single-phase π-type equivalent circuit model for blue Y-type LPG. (c) Single-phase instantaneous voltage of disharmonized VSCUs. (d) Characteristics analysis of oscillation with disharmonized VSCUs.

Figure 2(a) illustrates Y-type three-terminal LPG and two-terminal LPGs such as the LPG consisting of $VSCU_1$, $VSCU_2$, and line 1-2. Based on two-terminal LPGs, the oscillation caused by disharmony between two VSCUs and its adverse effect such as line power amplification effect have been previously explored. These two-terminal LPGs in previous research works cannot be used to analyze the impact of disharmony on loads, and there is a lack of research works on how multiple disharmonized VSCUs affect power flow of LPG, especially the load of non-active bus. The Y-type three-terminal LPG is capable of meeting the criteria for investigating the amplification effect as well as the swelling and sagging phenomena of load. Moreover, the analysis approach for the Y-type LPG can be easily expanded to star-type LPG with more than three VSCUs. In the following text, the disharmony oscillation at the grid side, and abnormal characteristics including swelling and sagging phenomena of load and amplification effect, are analyzed based on the blue Y-type LPG shown in Fig. 2(a).

In the Y-type LPG, buses 1, 2, and 3 are equipped with VSCUs, whose single-phase instantaneous voltages are denoted by $u_1(t)$, $u_2(t)$, and $u_3(t)$, respectively. Namely, these three buses are AC buses with the ability to actively control the voltage. Bus 0 is not equipped with VSCU, whose single-phase instantaneous voltage is denoted by $u_0(t)$. This bus is a non-active bus that lacks the ability of active voltage control and is connected to a load or a weak receiver-end power grid that can equate to an EL.

The single-phase π-type equivalent circuit model for the blue Y-type LPG is given in Fig. 2(b) considering the locality of disharmony and the output characteristics of VSCU. In Fig. 2, R_i, L_i, and C_i are the single-phase resistance, inductance, and ground capacitance of line i-0 ($i=1, 2, 3$), respectively; R_L and L_L are the equivalent load resistance and inductance of bus 0, respectively; $i_i(t)$ is the output instantaneous current of $VSCU_i$; $p_1(t)$ is the output single-phase instantaneous power of $VSCU_1$; $i_L(t)$ and $p_L(t)$ are the single-phase instantaneous current and power of load at bus 0, respectively; ω is harmony angular frequency corresponding to power frequency f and fundamental cycle T; $T_\oplus$ is the disharmony period which is obtained by (A11) in Appendix A, which corresponds to the disharmony frequency $f_\oplus$ and disharmony angular frequency $\omega_\oplus$.

Each VSCU is represented as a controlled voltage source (CVS) [28] at buses 1, 2, and 3 under the distributed synchronous GFM mode. Under SSOCs or QSSOCs, the output voltage and frequency of VSCU can be temporarily regarded as a constant value for a duration whose order is comparable to $T_\oplus$. Accordingly, the single-phase instantaneous voltages $u_i(t)$ for the same phase sequence (e.g., phase A) can be expressed as:

$$u_i(t)=U_{mi}\sin(\omega_i t+\varphi_i) \quad i=1,2,3 \tag{1}$$

where U_{mi} is the maximum value of $u_i(t)$; ω_i is the angular frequency with the corresponding period and frequency denoted by T_i and f_i, respectively; and φ_i is the initial phase of

$u_i(t)$. Among them, the absolute value of difference between f_i and f reflects the level of disharmony of VSCU.

The output frequency of each VSCU$_i$ is not exactly equal, which is influenced by multiple disharmony factors under SSOCs or QSSOCs. While a long-time disharmony between VSCUs occurs, whether it will have a harmful influence on power flow must be investigated thoroughly. The following section analyzes the abnormal behavior of load power and line power under DOCs based on Fig. 2.

III. Analysis of Abnormal Voltage and Power Characteristics of Non-active Bus with Disharmonized VSCUs

A. Non-active Bus Voltage

The equivalent circuit in Fig. 2 is a linear circuit, so the superposition theorem can be applied to derive $u_0(t)$, and the derivation process is given in Appendix A. $u_0(t)$ can be written as:

$$u_0(t)=U_{\mathrm{m0}}(t)\sin\psi_{\mathrm{v}}(t) \tag{2}$$

where $U_{\mathrm{m0}}(t)$ and $\psi_{\mathrm{v}}(t)$ are the time-varying peak and the time-varying phase of load voltage, respectively, which can be expressed by (A7) and (A8) in Appendix A. As shown in (2), $u_0(t)$ is a time-varying function of ω_1, ω_2, and ω_3. Under DOCs, $\omega_1\neq\omega_2\neq\omega_3$ and $u_0(t)$ will be abnormal in comparison to harmony operating conditions (HOCs). Disharmony will affect the quality of power supply to bus 0.

B. Abnormal Characteristics of Non-active Bus Voltage

Based on (2) and (A7) in Appendix A, the abnormal characteristics of non-active bus voltage under DOCs are analyzed from the following two aspects.

1) $U_{\mathrm{m0}}(t)$

When $\omega_1=\omega_2=\omega_3=\omega$, the load bus voltage peak $U_{\mathrm{m0}}^{[\mathrm{har}]}$ under HOCs can be derived from (A7) as:

$$U_{\mathrm{m0}}^{[\mathrm{har}]}=\left(\sum_{i=1}^{3}H_i^2+2H_1H_2\cos(\alpha_{\mathrm{v1}}-\alpha_{\mathrm{v2}})+2H_1H_3\cos(\alpha_{\mathrm{v1}}-\alpha_{\mathrm{v3}})+2H_2H_3\cos(\alpha_{\mathrm{v2}}-\alpha_{\mathrm{v3}})\right)^{\frac{1}{2}} \tag{3}$$

where H_i and $\alpha_{\mathrm{v}i}$ are the peak and initial phase of load bus voltage component i ($i=1, 2, 3$) of bus 0, respectively, which can be expressed by (A5) in Appendix A. As shown in (3), $U_{\mathrm{m0}}^{[\mathrm{har}]}$ is constant under HOCs.

When $\omega_1\neq\omega_2\neq\omega_3$, (A7) in Appendix A shows that $U_{\mathrm{m0}}(t)$ is a periodic function whose period is $T_{\oplus}$. Besides, the maximum value U_{m0max} and minimum value U_{m0min} of voltage peak, and their appearance time t_{m0max} and t_{m0min} can be caught by (A7) within a single period $T_{\oplus}$. Thus, the swelling and sagging indicators of the load bus voltage peak, $\kappa_{\mathrm{swe-v}}$ and $\kappa_{\mathrm{sag-v}}$, can be given as (4) and (5), respectively.

$$\kappa_{\mathrm{swe-v}}=\frac{U_{\mathrm{m0max}}}{U_{\mathrm{m0}}^{[\mathrm{har}]}}\times100\% \tag{4}$$

$$\kappa_{\mathrm{sag-v}}=\frac{U_{\mathrm{m0min}}}{U_{\mathrm{m0}}^{[\mathrm{har}]}}\times100\% \tag{5}$$

Similarly, $\kappa_{\mathrm{swe-c}}$ and $\kappa_{\mathrm{sag-c}}$ are the characteristic indicators that assess the effect of disharmony on load current peak. The more the deviation of indicators from 100% is, the more severe the impact of disharmony of VSCUs on load current peak will be, implying a more severe disharmony. Further analysis is presented in Section VI-B.

2) $\psi_{\mathrm{v}}(t)$ and Its Initial Phase

When $\omega_1=\omega_2=\omega_3=\omega$, the initial phase $\alpha_{\mathrm{v}\oplus}^{[\mathrm{har}]}$ of load bus voltage under HOCs can be derived from (A9) as:

$$\alpha_{\mathrm{v}\oplus}^{[\mathrm{har}]}=\mathrm{mod}\left(\mathrm{atan2}\left(\sum_{i=1}^{3}H_i\cos\alpha_{\mathrm{v}i},\sum_{i=1}^{3}H_i\sin\alpha_{\mathrm{v}i}\right),2\pi\right) \tag{6}$$

where mod(·, 2π) is the remainder function, which can convert "·" to the range of [0, 2π); and atan2(x, y) is the angle between (x, y) and the positive x-axis.

When $\omega_1\neq\omega_2\neq\omega_3$, let $\omega_{\oplus}$ be the angular frequency reference, and $\psi_{\mathrm{v}}(t)$ is given in another form by:

$$\psi_{\mathrm{v}}(t)=\mathrm{mod}(\omega_{\oplus}t+[(\omega_3-\omega_{\oplus})t+\alpha_{\mathrm{v}\oplus}(t)],2\pi)=\mathrm{mod}(\omega_{\oplus}t+\alpha_{\mathrm{v}\oplus}^{[\mathrm{dishar}]}(t),2\pi) \tag{7}$$

$$\alpha_{\mathrm{v}\oplus}^{[\mathrm{dishar}]}(t)=\mathrm{mod}((\omega_3-\omega_{\oplus})t+\mathrm{atan2}(H_1\cos(\omega_{13}t+\alpha_{\mathrm{v1}})+H_2\cos(\omega_{23}t+\alpha_{\mathrm{v2}})+H_3\cos\alpha_{\mathrm{v3}},H_1\sin(\omega_{13}t+\alpha_{\mathrm{v1}})+H_2\sin(\omega_{23}t+\alpha_{\mathrm{v2}})+H_3\sin\alpha_{\mathrm{v3}}),2\pi) \tag{8}$$

where $\alpha_{\mathrm{v}\oplus}^{[\mathrm{dishar}]}(t)$ is the initial phase of load bus voltage under DOCs, which is a time-varying function in the $\omega_{\oplus}$ reference frame, whose period is $T_{\oplus}$; and ω_{13} and ω_{23} are the differences between angular frequencies, which are given in (A10). When $t\in[0, T_{\oplus}]$, $\alpha_{\mathrm{v}\oplus}^{[\mathrm{dishar}]}(t)$ is no longer a constant, and $\alpha_{\mathrm{v}\oplus}^{[\mathrm{dishar}]}(0)=\alpha_{\mathrm{v}\oplus}^{[\mathrm{dishar}]}(T_{\oplus})$.

In summary, $U_{\mathrm{m0}}(t)$ and $\alpha_{\mathrm{v}\oplus}^{[\mathrm{dishar}]}(t)$ are both time-varying functions whose periods are $T_{\oplus}$. Under DOCs, $U_{\mathrm{m0}}(t)$ and $\alpha_{\mathrm{v}\oplus}^{[\mathrm{dishar}]}(t)$ are no longer constants in comparison to the HOCs, which causes $u_0(t)$ to be abnormal.

C. Abnormal Characteristics of Load Current and Power

In this subsection, the quality of power supply to bus 0 will be analyzed in terms of load current and power, respectively.

1) Abnormal Characteristics of Load Current

The load current phasor $\boldsymbol{I}_{\mathrm{L}(i)}(\omega_i)$ with only one CVS at bus i ($i=1, 2, 3$) derived from (A1) in Appendix A is given as:

$$\boldsymbol{I}_{\mathrm{L}(i)}(\omega_i)=\frac{k_{\mathrm{v}i}(\omega_i)\mathrm{e}^{\mathrm{j}\beta_{\mathrm{v}i}(\omega_i)}}{Z_{\mathrm{L}}(\omega_i)}\boldsymbol{U}_i(\omega_i)=k_{\mathrm{c}i}(\omega_i)\mathrm{e}^{\mathrm{j}\beta_{\mathrm{c}i}(\omega_i)}\boldsymbol{U}_i(\omega_i) \tag{9}$$

where $\boldsymbol{U}_i(\omega_i)$ is the single-phase voltage phasor of bus i when the system frequency is f_i; and $k_{\mathrm{c}i}(\omega_i)$ and $\beta_{\mathrm{c}i}(\omega_i)$ are the module and angle of $k_{\mathrm{v}i}(\omega_i)\mathrm{e}^{\mathrm{j}\beta_{\mathrm{v}i}(\omega_i)}/Z_{\mathrm{L}}(\omega_i)$, respectively.

Let

$$\begin{cases}J_i=k_{\mathrm{c}i}(\omega_i)U_{\mathrm{m}i}\\ \alpha_{\mathrm{c}i}=\varphi_i+\beta_{\mathrm{c}i}(\omega_i)\end{cases} \tag{10}$$

where J_i and $\alpha_{\mathrm{c}i}$ are the module and angle of load current component i, respectively. Thus, the single-phase instantaneous current $i_{\mathrm{L}}(t)$ of the EL at bus 0 with all the CVSs is given as:

$$i_{\mathrm{L}}(t)=I_{\mathrm{Lm}}(t)\sin\psi_{\mathrm{c}}(t) \tag{11}$$

where the load current peak $I_{\mathrm{Lm}}(t)$, the time-varying phase $\psi_{\mathrm{c}}(t)$, and initial phase $\alpha_{\mathrm{c}\oplus}(t)$ of load current are given in

(12) and (13).

$$I_{\mathrm{Lm}}(t)=\left(\sum_{i=1}^{3}J_i^2+2J_1J_2\cos(\omega_{12}t+\alpha_{\mathrm{c1}}-\alpha_{\mathrm{c2}})+2J_1J_3\cos(\omega_{13}t+\alpha_{\mathrm{c1}}-\alpha_{\mathrm{c3}})+2J_2J_3\cos(\omega_{23}t+\alpha_{\mathrm{c2}}-\alpha_{\mathrm{c3}})\right)^{\frac{1}{2}} \tag{12}$$

$$\begin{cases}\psi_{\mathrm{c}}(t)=\mathrm{mod}(\omega_3 t+\alpha_{\mathrm{c}\oplus}(t),2\pi)\\ \alpha_{\mathrm{c}\oplus}(t)=\mathrm{mod}(\mathrm{atan2}(J_1\cos(\omega_{13}t+\alpha_{\mathrm{c1}})+J_2\cos(\omega_{23}t+\alpha_{\mathrm{c2}})+\\ \qquad J_3\cos\alpha_{\mathrm{c3}},J_1\sin(\omega_{13}t+\alpha_{\mathrm{c1}})+J_2\sin(\omega_{23}t+\alpha_{\mathrm{c2}})+\\ \qquad J_3\sin\alpha_{\mathrm{c3}}),2\pi)\end{cases} \tag{13}$$

As shown in (11)-(13) and Appendix B, $I_{\mathrm{Lm}}(t)$ and $\alpha_{\mathrm{c}\oplus}^{[\mathrm{dishar}]}(t)$ are both periodic functions, whose periods are $T_\oplus$, since (11)-(13) resemble (A6)-(A9) in Appendix A in form. Under DOCs, $I_{\mathrm{Lm}}(t)$ and $\alpha_{\mathrm{c}\oplus}^{[\mathrm{dishar}]}(t)$ are no longer constants in comparison to the HOCs, leading to the abnormal value of $i_{\mathrm{L}}(t)$.

Furthermore, the maximum value I_{Lmmax} and the minimum value I_{Lmmin} of load current peak, and their appearance time t_{Lmmax} and t_{Lmmin} can be caught by (12) within a single period $T_\oplus$. Thus, the swelling and sagging indicators of load current peak, $\kappa_{\mathrm{swe-c}}$ and $\kappa_{\mathrm{sag-c}}$, can be given as (14) and (15), respectively.

$$\kappa_{\mathrm{swe-c}}=\frac{I_{\mathrm{Lmmax}}}{I_{\mathrm{Lm}}^{[\mathrm{har}]}}\times 100\% \tag{14}$$

$$\kappa_{\mathrm{sag-c}}=\frac{I_{\mathrm{Lmmin}}}{I_{\mathrm{Lm}}^{[\mathrm{har}]}}\times 100\% \tag{15}$$

where $I_{\mathrm{Lm}}^{[\mathrm{har}]}$ is the load current peak under HOCs, which is given in (A12).

$\kappa_{\mathrm{swe-c}}$ and $\kappa_{\mathrm{sag-c}}$ are the characteristic indicators that assess the effect of disharmony on load current peak. The more the deviation of indicators from 100% is, the more severe the impact of disharmony of VSCUs on load current peak is, implying a more severe disharmony. Further analysis is presented in Section VI-B.

2) Abnormal Characteristics of Load Power

Multiplying (2) by (11) yields $p_{\mathrm{L}}(t)$:

$$p_{\mathrm{L}}(t)=0.5P_{\mathrm{Lm}}(t)(\cos(\alpha_{\mathrm{v}\oplus}^{[\mathrm{dishar}]}(t)-\alpha_{\mathrm{c}\oplus}^{[\mathrm{dishar}]}(t))-\cos(2\omega_\oplus t+\alpha_{\mathrm{v}\oplus}^{[\mathrm{dishar}]}(t)+\alpha_{\mathrm{c}\oplus}^{[\mathrm{dishar}]}(t))) \tag{16}$$

$$P_{\mathrm{Lm}}(t)=U_{\mathrm{m0}}(t)I_{\mathrm{Lm}}(t) \tag{17}$$

where $P_{\mathrm{Lm}}(t)$ is the time-varying peak of $p_{\mathrm{L}}(t)$.

The periods of $\alpha_{\mathrm{v}\oplus}^{[\mathrm{dishar}]}(t)\pm\alpha_{\mathrm{c}\oplus}^{[\mathrm{dishar}]}(t)$ and $P_{\mathrm{Lm}}(t)$ are $T_\oplus$ under DOCs because the periods of $\alpha_{\mathrm{v}\oplus}^{[\mathrm{dishar}]}(t)$, $\alpha_{\mathrm{c}\oplus}^{[\mathrm{dishar}]}(t)$, $U_{\mathrm{m0}}(t)$, and $I_{\mathrm{Lm}}(t)$ are $T_\oplus$. Given that the period of $\cos(2\omega_\oplus t)$ is $T_\oplus/2$, the period of $p_{\mathrm{L}}(t)$ is $T_\oplus$.

Correspondingly, when $\omega_1=\omega_2=\omega_3=\omega$, the single-phase instantaneous power $p_{\mathrm{L}}^{[\mathrm{har}]}(t)$ of the EL under HOCs is:

$$p_{\mathrm{L}}^{[\mathrm{har}]}(t)=0.5U_{\mathrm{m0}}^{[\mathrm{har}]}I_{\mathrm{Lm}}^{[\mathrm{har}]}(\cos(\alpha_{\mathrm{v}\oplus}^{[\mathrm{har}]}-\alpha_{\mathrm{c}\oplus}^{[\mathrm{har}]})-\cos(2\omega t+\alpha_{\mathrm{v}\oplus}^{[\mathrm{har}]}+\alpha_{\mathrm{c}\oplus}^{[\mathrm{har}]})) \tag{18}$$

As shown in (18), the period of $p_{\mathrm{L}}^{[\mathrm{har}]}(t)$ is $T/2$, which is unequal to the period $T_\oplus$ of $P_{\mathrm{Lm}}(t)$. In general, $T/2 \ll T_\oplus$. The average power $\bar{P}_{\mathrm{L}}(t)$ is significantly lower than the average power $\bar{P}_{\mathrm{L}}^{[\mathrm{har}]}$ during some intervals of $T/2$ length within the time window of $T_\oplus$ length. As a consequence, there is a sharp decline in load supply level. The average power $\bar{P}_{\mathrm{L}}(t)$ under DOCs and average power $\bar{P}_{\mathrm{L}}^{[\mathrm{har}]}$ under HOCs are expressed as:

$$\bar{P}_{\mathrm{L}}(t)=\frac{2}{T}\int_t^{t+T/2}p_{\mathrm{L}}(t)\mathrm{d}t \tag{19}$$

$$\bar{P}_{\mathrm{L}}^{[\mathrm{har}]}=\frac{2}{T}\int_t^{t+T/2}p_{\mathrm{L}}^{[\mathrm{har}]}(t)\mathrm{d}t=0.5U_{\mathrm{m0}}^{[\mathrm{har}]}I_{\mathrm{Lm}}^{[\mathrm{har}]}\cos(\alpha_{\mathrm{v}\oplus}^{[\mathrm{har}]}-\alpha_{\mathrm{c}\oplus}^{[\mathrm{har}]}) \tag{20}$$

Additionally, the maximum value $\bar{P}_{\mathrm{Lmax}}$ and the minimum value $\bar{P}_{\mathrm{Lmin}}$ of average power $\bar{P}_{\mathrm{L}}(t)$, and their appearance time t_{Lmax} and t_{Lmin} can be caught by (19) within a single period $T_\oplus$. Thus, the sagging indicator of average load power can be given as:

$$\kappa_{\mathrm{sag-p}}=\frac{\bar{P}_{\mathrm{Lmin}}}{\bar{P}_{\mathrm{L}}^{[\mathrm{har}]}}\times 100\% \tag{21}$$

$\kappa_{\mathrm{swe-p}}$ is a characteristic indicator that assesses the effect of disharmony on the average load power. The more the deviation of the indicator from 100% is, the more severe the impact of disharmony of VSCUs on the average load power will be, implying a more severe disharmony. Further analysis will be presented in Section VI-B.

IV. Characteristics Analysis of Line Current Oscillation with Disharmonized VSCUs

A. Non-active Bus Voltage

In this subsection, the time-varying characteristics of line current will be analyzed in terms of $i_1(t)$. For the equivalent circuit with the CVS at bus 1, 2, or 3, the current phasors of line 1-0 $\boldsymbol{I}_{1(i)}(\omega_i)$ are derived by superposition theorem as:

$$\boldsymbol{I}_{1(i)}(\omega_i)=\begin{cases}\mathrm{j}\omega_1C_1\boldsymbol{U}_1(\omega_1)+Y_1(\omega_1)(\boldsymbol{U}_1(\omega_1)-\boldsymbol{U}_{0(1)}(\omega_1)) & i=1\\ -Y_1(\omega_2)\boldsymbol{U}_{0(2)}(\omega_2) & i=2\\ -Y_1(\omega_3)\boldsymbol{U}_{0(3)}(\omega_2) & i=3\end{cases} \tag{22}$$

where the branch admittance $Y_1(\omega_i)$ is the function of ω_i; and $\boldsymbol{U}_{0(1)}(\omega_1)$ is the single-phase voltage phasor of bus 0 when the system frequency is f_1, which is given in (A1). $Y_1(\omega_i)=1/Z_1(\omega_i)$, and $Z_1(\omega_i)$ is the impedance of line 1-0 when the system frequency is f_i.

Let

$$\begin{cases}\lambda_{\mathrm{c1}}(\omega_1)\,\mathrm{e}^{\mathrm{j}\phi_{\mathrm{c1}}(\omega_1)}=\mathrm{j}\omega_1C_1+Y_1(\omega_1)-Y_1(\omega_1)k_{\mathrm{v1}}(\omega_1)\mathrm{e}^{\mathrm{j}\beta_{\mathrm{v1}}(\omega_1)}\\ \lambda_{\mathrm{c2}}(\omega_2)\,\mathrm{e}^{\mathrm{j}\phi_{\mathrm{c2}}(\omega_2)}=-Y_1(\omega_2)k_{\mathrm{v2}}(\omega_2)\mathrm{e}^{\mathrm{j}\beta_{\mathrm{v2}}(\omega_2)}\\ \lambda_{\mathrm{c3}}(\omega_3)\,\mathrm{e}^{\mathrm{j}\phi_{\mathrm{c3}}(\omega_3)}=-Y_1(\omega_3)k_{\mathrm{v3}}(\omega_3)\mathrm{e}^{\mathrm{j}\beta_{\mathrm{v3}}(\omega_3)}\end{cases} \tag{24}$$

where $\lambda_{ci}(\omega_i)$ and $\phi_{ci}(\omega_i)$ are the module and angle, respectively.

Equation (22) can be simplified as:

$$\boldsymbol{I}_{1(i)}(\omega_i)=\begin{cases}\lambda_{\mathrm{c1}}(\omega_1)\,\mathrm{e}^{\mathrm{j}\phi_{\mathrm{c1}}(\omega_1)}\boldsymbol{U}_1(\omega_1) & i=1\\ \lambda_{\mathrm{c2}}(\omega_2)\,\mathrm{e}^{\mathrm{j}\phi_{\mathrm{c2}}(\omega_2)}\boldsymbol{U}_2(\omega_2) & i=2\\ \lambda_{\mathrm{c3}}(\omega_3)\,\mathrm{e}^{\mathrm{j}\phi_{\mathrm{c3}}(\omega_3)}\boldsymbol{U}_3(\omega_3) & i=3\end{cases} \tag{23}$$

Let

$$\begin{cases}M_i=\lambda_{ci}U_{\mathrm{m}i}\\ \gamma_i=\varphi_i+\phi_{ci}\end{cases}\quad i=1,2,3 \tag{25}$$

where M_i and γ_i are the module and angle of current compo-

nent i of line 1-0, respectively.

Thus, the current of line 1-0 $i_1(t)$ is:

$$i_1(t)=I_{1\mathrm{m}}(t)\sin\delta(t) \tag{26}$$

where the line current peak $I_{1\mathrm{m}}(t)$, time-varying phase $\delta(t)$, and initial phase $\gamma_{\oplus}(t)$ of line current are given in (27) and (28).

$$I_{1\mathrm{m}}(t)=\left(\sum_i^3 M_i^2+2M_1M_2\cos(\omega_{12}t+\gamma_1-\gamma_2)+2M_1M_3\cos(\omega_{13}t+\gamma_1-\gamma_3)+2M_2M_3\cos(\omega_{23}t+\gamma_2-\gamma_3)\right)^{\frac{1}{2}} \tag{27}$$

$$\begin{cases}\delta(t)=\mathrm{mod}(\omega_3 t+\gamma_{\oplus}(t),2\pi)\\ \gamma_{\oplus}(t)=\mathrm{mod}(\mathrm{atan2}(M_1\cos(\omega_{13}t+\gamma_1)+M_2\cos(\omega_{23}t+\gamma_2)+M_3\cos\gamma_3, M_1\sin(\omega_{13}t+\gamma_1)+M_2\sin(\omega_{23}t+\gamma_2)+M_3\sin\gamma_3),2\pi)\end{cases} \tag{28}$$

B. Amplification Effect of Oscillation Peak of Line Current

As shown in (26) and Appendix C, $I_{1\mathrm{m}}(t)$ and $\gamma_{\oplus}^{[\mathrm{dishar}]}(t)$ are both periodic functions, whose periods are $T_{\oplus}$, since (26)-(28) resemble (2) and (B1) in Appendix B in form. Under DOCs, $I_{\mathrm{Lm}}(t)$ and $\alpha_{\mathrm{c}\oplus}^{[\mathrm{dishar}]}(t)$ are no longer constants in comparison to the HOCs, leading to the abnormal value of $i_{\mathrm{L}}(t)$. This results in peak amplification and reduction effects of $i_1(t)$. Especially, the peak amplification is likely to increase the probability of overload in the transmission line.

In addition, the maximum peak $I_{1\mathrm{mmax}}$ and minimum value $I_{1\mathrm{mmin}}$ of $I_{1\mathrm{m}}(t)$, and their appearance time $t_{1\mathrm{mmax}}$ and $t_{1\mathrm{mmin}}$ can be caught by (27) within a single period $T_{\oplus}$. Thus, the current peak gain K_{cp} can be given as:

$$K_{\mathrm{cp}}=\frac{I_{1\mathrm{mmax}}}{I_{1\mathrm{m}}^{[\mathrm{har}]}} \tag{29}$$

where $I_{1\mathrm{m}}^{[\mathrm{har}]}$ is the line current peak under HOCs, which is given in (A16).

K_{cp} is the key indicator that assesses the amplification effect of line current oscillation peak before and after disharmony. The larger K_{cp} is, the more serious the line current will be influenced by the disharmony of VSCUs, implying a higher probability of unstable operation on the transmission line and more severe disharmony. Further analysis will be presented in Section VI-B.

V. Characteristics Analysis of Line Power Oscillation with Disharmonized VSCUs

A. Formula for Line Power

In this subsection, the time-varying characteristics of line power will be analyzed in terms of $p_1(t)$. Multiplying (1) by (26) yields $p_1(t)$ as:

$$p_1(t)=0.5P_{1\mathrm{m}}(t)(\cos((\omega_1-\omega_{\oplus})t+\varphi_1-\gamma_{\oplus}^{[\mathrm{dishar}]}(t))-\cos((\omega_1+\omega_{\oplus})t+\varphi_1+\gamma_{\oplus}^{[\mathrm{dishar}]}(t))) \tag{30}$$

$$P_{1\mathrm{m}}(t)=U_{\mathrm{m}1}I_{1\mathrm{m}}(t) \tag{31}$$

where $P_{1\mathrm{m}}(t)$ is the time-varying peak of $p_1(t)$.

As shown in (30), $p_1(t)$ consists of two time-varying components. Although the time-varying peaks of both components in (30) are equal to $0.5U_{\mathrm{m}1}I_{1\mathrm{m}}(t)$, their angular frequencies and initial phases are different. Therefore, the maximum peak $P_{1\mathrm{m}}(t)$ is not equal to $0.5U_{\mathrm{m}1}I_{1\mathrm{m}}(t)$.

B. Amplification Effect of Oscillation Peak of Line Power

When $\omega_1\neq\omega_2\neq\omega_3$, the average power of $p_1(t)$ in each period T_1 can be derived from (30) as:

$$\bar{P}_1(t)=\frac{1}{T_1}\int_t^{t+T_1}p_1(\tau)\mathrm{d}\tau \tag{32}$$

According to (32), the maximum value $\bar{P}_{1\mathrm{max}}$ and the minimum value $\bar{P}_{1\mathrm{min}}$ of $\bar{P}_1(t)$, and their appearance time $\tau_{1\mathrm{max}}$ and $\tau_{1\mathrm{min}}$ can be obtained.

When $\omega_1=\omega_2=\omega_3=\omega$, the single-phase instantaneous line power $p_1^{[\mathrm{har}]}(t)$ under HOCs can be derived from (30) as:

$$p_1^{[\mathrm{har}]}(t)=0.5U_{\mathrm{m}1}I_{1\mathrm{m}}^{[\mathrm{har}]}(\cos(\varphi_1-\gamma_{\oplus}^{[\mathrm{har}]})-\cos(2\omega t+\varphi_1+\gamma_{\oplus}^{[\mathrm{har}]})) \tag{33}$$

where $\gamma_{\oplus}^{[\mathrm{har}]}$ is the initial phase of current of line 1-0 under HOCs.

The maximum value $P_{1\mathrm{max}}^{[\mathrm{har}]}$ and the minimum value $P_{1\mathrm{min}}^{[\mathrm{har}]}$ of $p_1^{[\mathrm{har}]}(t)$ can be rewritten as:

$$\begin{cases}P_{1\mathrm{max}}^{[\mathrm{har}]}=0.5U_{\mathrm{m}1}I_{1\mathrm{m}}^{[\mathrm{har}]}(\cos(\varphi_1-\gamma_{\oplus}^{[\mathrm{har}]})+1)\\ P_{1\mathrm{min}}^{[\mathrm{har}]}=0.5U_{\mathrm{m}1}I_{1\mathrm{m}}^{[\mathrm{har}]}(\cos(\varphi_1-\gamma_{\oplus}^{[\mathrm{har}]})-1)\end{cases} \tag{34}$$

The average power of $p_1^{[\mathrm{har}]}(t)$ during one period T under HOCs can be obtained by (33) as:

$$\bar{P}_1^{[\mathrm{har}]}=0.5U_{\mathrm{m}1}I_{1\mathrm{m}}^{[\mathrm{har}]}\cos(\varphi_1-\gamma_{\oplus}^{[\mathrm{har}]}) \tag{35}$$

In addition, the maximum value $P_{1\mathrm{mmax}}$ and the minimum value $P_{1\mathrm{mmin}}$ of $P_{1\mathrm{m}}(t)$, and their appearance time $\tau_{1\mathrm{mmax}}$ and $\tau_{1\mathrm{mmin}}$ can be caught by (31), where $t\in[0, T_{\oplus}]$. Thus, the power peak gain K_{pp} and average power gain $\overline{K}_{\mathrm{pp}}$ can be given as:

$$K_{\mathrm{pp}}=\frac{P_{1\mathrm{mmax}}}{P_{1\mathrm{max}}^{[\mathrm{har}]}} \tag{36}$$

$$\overline{K}_{\mathrm{pp}}=\frac{\bar{P}_{1\mathrm{max}}}{\bar{P}_1^{[\mathrm{har}]}} \tag{37}$$

K_{pp} and $\overline{K}_{\mathrm{pp}}$ are the key indicators that assess the amplification effect of power oscillation before and after disharmony, respectively. The larger K_{pp} and $\overline{K}_{\mathrm{pp}}$ are, the more seriously the disharmonized VSCUs will influence the line power, suggesting a higher likelihood of overload in the transmission line and more severe disharmony. Further analysis will be presented in Section VI-B.

So far, comprehensive analyses have been conducted on the abnormal characteristics of voltage, current, power, and their key indicators. On this basis, we will further quantify the influence of relevant parameters on the disharmony oscillation in the next section.

VI. Case Study

A. Parameters of Test System

Let the voltage level and reference voltage of Y-type three-terminal LPG in Fig. 2 be 500 kV. The harmony frequency is 50 Hz. Other parameters of the equivalent circuit model are given in Table I.

In addition, let the calculation time-step t_{step} be 1 ms and the frequency-step (minimum frequency resolution) f_{step} be 0.001 Hz for the simulation.

TABLE I
PARAMETERS OF EQUIVALENT CIRCUIT MODEL

Location	Parameter	Value
VSCU at bus 1	Single-phase root-mean-square voltage U_1	1.016379 p.u.
	Initial phase φ_1	7.619244°
	Frequency f_1	50.010 Hz
VSCU at bus 2	Single-phase root-mean-square voltage U_2	0.995 p.u.
	Initial phase φ_2	–3.000°
	Frequency f_2	49.990 Hz
VSCU at bus 3	Single-phase root-mean-square voltage U_3	1.000 p.u.
	Initial phase φ_3	–4.000°
	Frequency f_3	50.005 Hz
Load at bus 0 under HOC	Single-phase load power P_0	200 MW
	Power factor $\cos\varphi_0$	0.95
	Voltage phasor $\boldsymbol{U}_0$	1.0 p.u.∠0°
Lines 1-0, 2-0, and 3-0	Resistance of unit-length line r_0	0.023543 Ω/km
	Inductance of unit-length line l_0	0.860016 mH/km
	Capacitance of unit-length line c_0	0.013100 μF/km
	Length of line 1-0 d_1	100 km
	Length of line 2-0 d_2	150 km
	Length of line 3-0 d_3	200 km

B. Simulation Results

1) Disharmony Period

The integer outcomes of f_1/f_{step}, f_2/f_{step}, and f_3/f_{step} are 50010, 49990, and 50005, respectively, and their greatest common divisor is 5. Thus, $f_{\oplus}=5f_{\text{step}}=0.005$ Hz and $T_{\oplus}=200$ s.

2) Analysis Results of Load Flow Under DOC

1) Abnormal characteristics of load bus voltage

① Voltage peak of non-active bus

Figure 3(a) illustrates the single-phase instantaneous voltage and its peak value of bus 0 under DOC. The periods of $u_0(t)$ and $U_{\text{m0}}(t)$ are 200 s. The values of U_{m0max} and U_{m0min}, their appearance time, and swelling and sagging indicators can be found in Table II.

The above results indicate that the disharmony among the three VSCUs causes the voltage amplitude of non-active bus to be no longer constant. Specifically, the swelling and sagging degrees of voltage peak reach the maximum at t_{m0max} and t_{m0min}, respectively, which seriously affect the load capacity of bus 0.

② Initial phase of load voltage

Figure 3(b) and (c) shows the initial phase of load voltage in the ω_3 and $\omega_{\oplus}$ reference frame under DOC. In comparison to $\alpha_{\text{v}\oplus}^{[\text{har}]}=6.283284$ rad, the periods of $\alpha_{\text{v}\oplus}^{[\text{dishar}]}(t)$ and $\alpha_{\text{v}\oplus}(t)$ are $T_{\oplus}$, indicating that disharmony leads to periodic property of the initial phase of load voltage.

2) Abnormal characteristics of load current

① Current peak of non-active bus

Figure 4(a) illustrates the single-phase instantaneous current and its peak value of the EL at bus 0 under DOC. The period of $i_{\text{L}}(t)$ and $I_{\text{Lm}}(t)$ is 200 s. The values of I_{Lmmax}, I_{Lmmin}, their appearance time, and swelling and sagging indicators can be found in Table III.

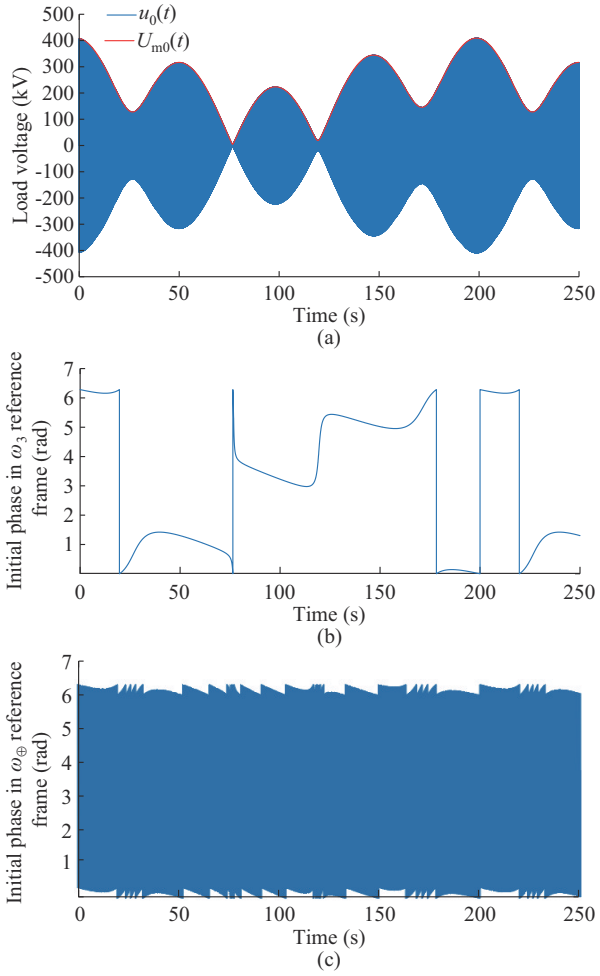

Fig. 3. Single-phase instantaneous voltage of bus 0, peak value, and initial phase under DOC. (a) Single-phase instantaneous voltage and its peak value. (b) Initial phase in ω_3 reference frame. (c) Initial phase in $\omega_{\oplus}$ reference frame.

TABLE II
VOLTAGE PEAK AND CHARACTERISTIC INDICATORS OF NON-ACTIVE BUS

Condition	Parameter	Value
Under DOC	The maximum load voltage peak under DOC U_{m0max}	409.284 kV
	Appearance time of the maximum of load voltage peak under DOC t_{m0max}	198.695 s
	The minimum load voltage peak under DOC U_{m0min}	5.065 kV
	Appearance time of the minimum of load voltage peak under DOC t_{m0min}	76.720 s
Under HOC	Load voltage peak under HOC $U_{\text{m0}}^{[\text{har}]}$	408.249 kV
Indicators	Swelling indicator of load voltage peak $\kappa_{\text{swe-v}}$	100.25%
	Sagging indicator of load voltage peak $\kappa_{\text{sag-v}}$	1.24%

The above results indicate that the disharmony among the three VSCUs causes the current amplitude of the non-active bus to be no longer constant. Specifically, the swelling and sagging degrees of the current peak reach the maximum at t_{Lmmin} and t_{Lmmax}, respectively, which seriously affect the load capacity and stability of this bus.

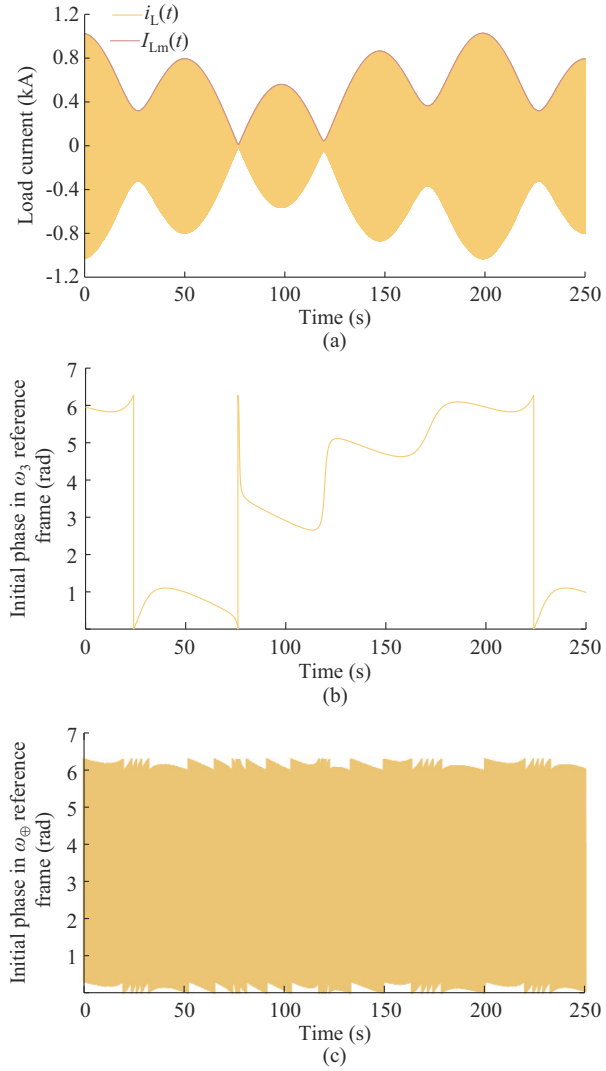

Fig. 4. Single-phase instantaneous current and its peak value of EL at bus 0 and initial phase of single-phase instantaneous current of bus 0 under DOC. (a) Single-phase instantaneous current and its peak value. (b) Initial phase in ω_3 reference frame. (c) Initial phase in $\omega_\oplus$ reference frame.

TABLE III
CURRENT PEAK AND CHARACTERISTIC INDICATORS OF EL

Condition	Parameter	Value
Under DOC	The maximum load current peak under DOC I_{Lmmax}	1.034 kA
	Appearance time of the maximum of load current peak under DOC t_{Lmmax}	198.696 s
	The minimum load current peak under DOC I_{Lmmin}	0.013 kA
	Appearance time of the minimum of load current peak under DOC t_{Lmmin}	76.721 s
Under HOC	Load current peak under HOC $I_{Lm}^{[har]}$	1.031 kA
Indicators	Swelling indicator of load current peak κ_{swe-c}	100.25%
	Sagging indicator of load current peak κ_{sag-c}	1.24%

② Initial phase of load current

Figure 4(b) and (c) shows the initial phases of load current in the ω_3 and $\omega_\oplus$ reference frames under DOC. In comparison to $\alpha_{c\oplus}^{[har]}=5.965606$ rad, the periods of $\alpha_{c\oplus}^{[dishar]}(t)$ and $\alpha_{c\oplus}(t)$ are $T_\oplus$, indicating that the disharmony leads to periodic property of the initial phase of load current.

3) Abnormal characteristics of load power

Figure 5 illustrates the single-phase instantaneous load power and its average value of bus 0 under DOC. The periods of $p_L(t)$ and $\bar{P}_L(t)$ are 200 s. The values of $\bar{P}_{Lmax}$ and $\bar{P}_{Lmin}$, their appearance time, and sagging indicator for average power can be found in Table IV.

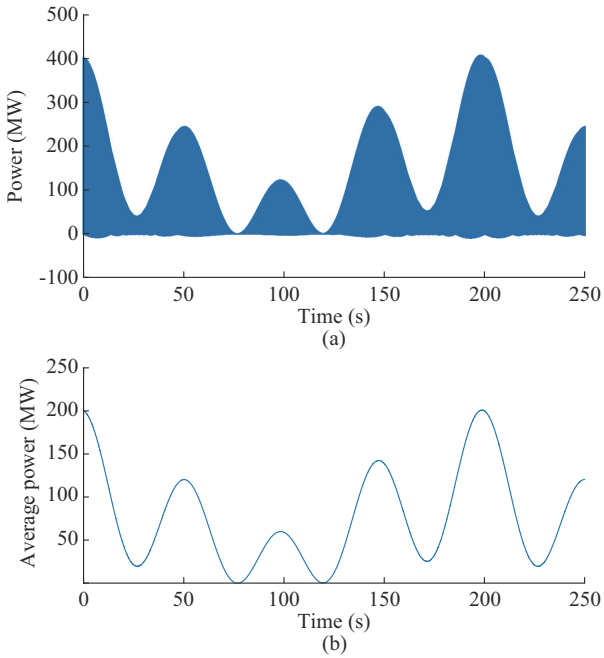

Fig. 5. Single-phase instantaneous power and its average value of bus 0 under DOC. (a) Single-phase instantaneous power. (b) Average power.

TABLE IV
AVERAGE POWER AND CHARACTERISTIC INDICATORS OF EL

Condition	Parameter	Value
Under DOC	The maximum average power of EL under DOC $\bar{P}_{Lmax}$	201.025 MW
	Appearance time of the maximum of average power of EL under DOC t_{Lmax}	198.686 s
	The minimum average power of EL under DOC $\bar{P}_{Lmin}$	0.031 MW
	Appearance time of the minimum of average power of EL under DOC t_{Lmin}	76.721 s
Under HOC	Average power of EL under HOC $\bar{P}_L^{[har]}$	199.999 MW
Indicator	Sagging indicator for average power of EL κ_{sag-p}	0.02%

Table IV demonstrates that the average power of the EL at bus 0 fluctuates significantly between 0 s and 200 s. The load capacity of bus 0 declines to a lower level at around 26.7 s, 76.7 s, 126.7 s, and 176.7 s, and almost to zero at around 76.721 s, which results in a temporary loss of load capacity.

3) Analysis Results of Line Current Flow Under DOC

1) Abnormal characteristics of line current

① Current peak of line 1-0

Figure 6(a) illustrates the single-phase instantaneous current

of line 1-0 and its peak value under DOC. The periods of $i_1(t)$ and $I_{1m}(t)$ are 200 s. The values of I_{1mmax} and I_{1mmin}, their appearance time, and current peak gain can be found in Table V.

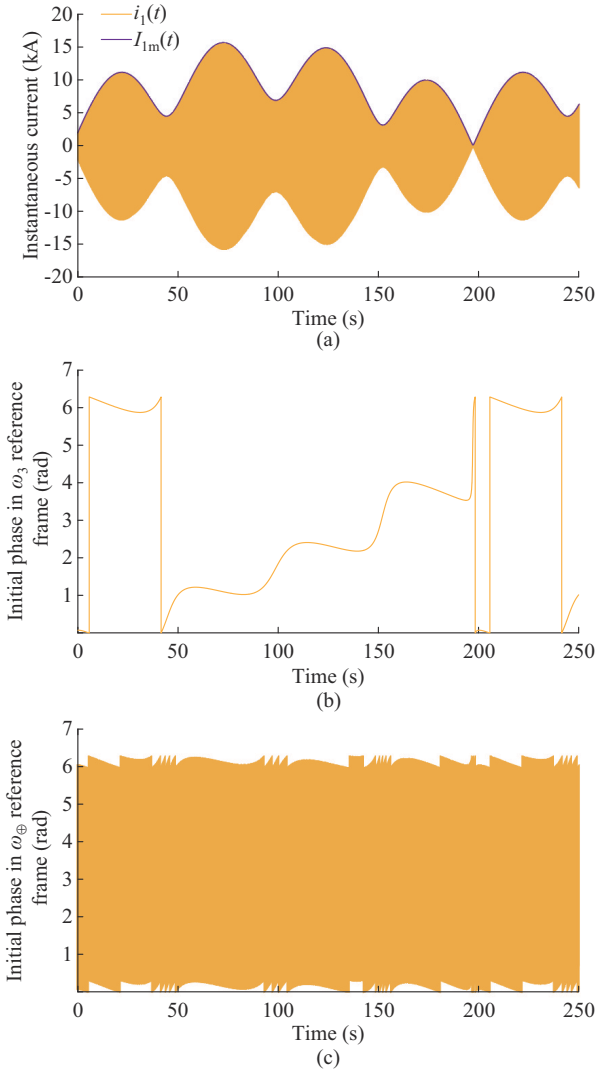

Fig. 6. Single-phase instantaneous current from $VSCU_1$ on line 1-0 and its initial phase under DOC. (a) Single-phase instantaneous current. (b) Initial phase in ω_3 reference frame. (c) Initial phase in $\omega_\oplus$ reference frame.

TABLE V
CURRENT PEAK OF LINE 1-0 AND DISTORTION INDICATORS

Condition	Parameter	Value
Under DOC	The maximum current peak of line 1-0 under DOC I_{1mmax}	15.782 kA
	Appearance time of the maximum current peak of line 1-0 under DOC t_{Lmax}	72.611 s
	The minimum current peak of line 1-0 under DOC I_{1mmin}	0.180 kA
	Appearance time of the minimum current peak of line 1-0 under DOC t_{Lmin}	197.090 s
Under HOC	Current peak of line 1-0 under HOC $I_{1m}^{[har]}$	199.999 kA
Indicator	Sagging indicator for average power of EL κ_{sag-p}	0.02%

The above results indicate that the disharmony among the three VSCUs will cause an increase in the line current peak several times.

② Initial phase of current of line 1-0

Figure 6(b) and (c) shows the initial phases of current of line 1-0 in the ω_3 and $\omega_\oplus$ reference frames under DOC, respectively. In comparison to $\gamma_\oplus^{[har]}=0.075068$ rad, the periods of $\gamma_\oplus^{[dishar]}(t)$ and $\gamma_\oplus(t)$ are $T_\oplus$, indicating that the disharmony leads to periodic property of the initial phase of current of line 1-0.

2) Abnormal characteristics of line power

Figure 7(a) illustrates the single-phase instantaneous power of line 1-0 under HOC. The values of $P_{1max}^{[har]}$, $P_{1min}^{[har]}$, and $\bar{P}_1^{[har]}$ can be found in Table VI. Figure 7(b)-(d) presents the single-phase instantaneous power of line 1-0 under DOC. The periods of $p_1(t)$, $P_{1m}(t)$, and $\bar{P}_1(t)$ are 200 s. The values of P_{1mmax}, P_{1mmin} and their appearance time, $\bar{P}_{1max}$, $\bar{P}_{1min}$ and their appearance time, as well as their characteristic indicators can be found equally in Table VI.

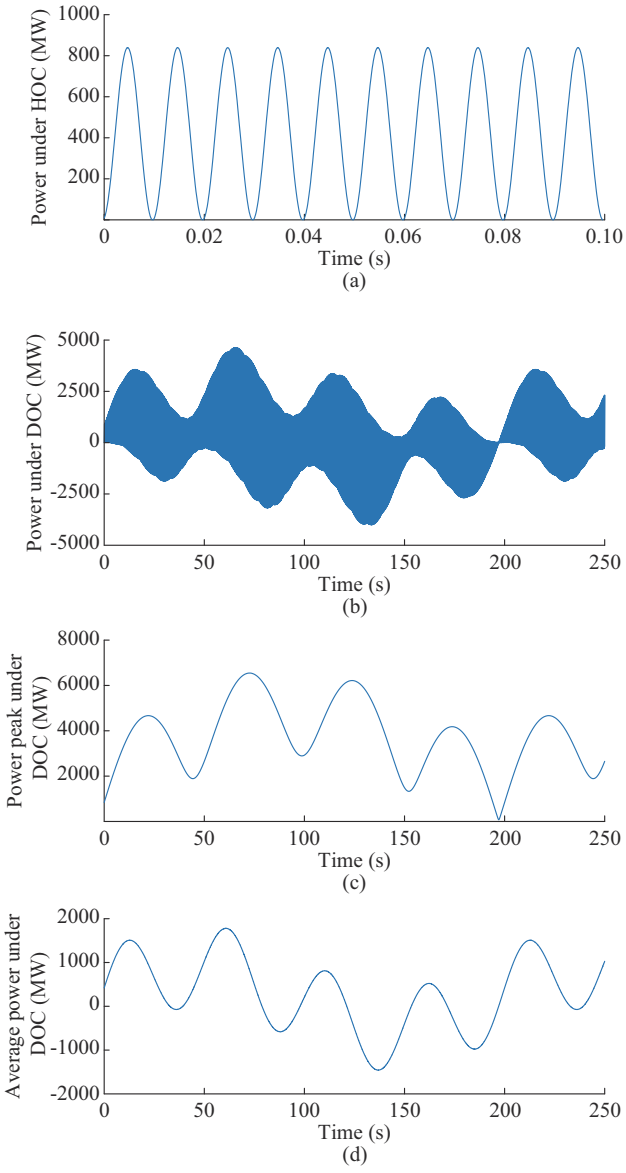

Fig. 7. Single-phase instantaneous power, power peak, and average power from $VSCU_1$ of line 1-0. (a) Single-phase instantaneous power under HOC. (b) Single-phase instantaneous power under DOC. (c) Power peak under DOC. (d) Average power under DOC.

TABLE VI
POWER PEAK AND AVERAGE POWER FROM $VSCU_1$ ON LINE 1-0 AND DISTORTION INDICATORS UNDER DOC AND HOC

Condition	Parameter	Value
Under DOC	The maximum power peak of line 1-0 under DOC P_{1mmax}	6548.542 MW
	Appearance time of the maximum power peak of line 1-0 under DOC τ_{1mmax}	72.611 s
	The minimum power peak of line 1-0 under DOC P_{1mmin}	74.580 MW
	Appearance time of the minimum power peak of line 1-0 under DOC τ_{1mmin}	197.090 s
	The maximum average power of line1-0 under DOC $\bar{P}_{1max}$	1781.211 MW
	Appearance time of the maximum average power of line1-0 under DOC τ_{1max}	60.774 s
	The minimum average power of line1-0 under DOC $\bar{P}_{1min}$	−1456.438 MW
	Appearance time of the minimum average power of line1-0 under DOC τ_{1min}	138.865 s
Under HOC	The maximum power of line 1-0 under HOC $P_{1max}^{[har]}$	839.286 MW
	The minimum power of line 1-0 under HOC $P_{1min}^{[har]}$	−0.704 MW
	Average power of line 1-0 under HOC $\bar{P}_{l}^{[har]}$	419.291 MW
Gains	Power peak gain K_{pp}	7.803
	Average power gain $\overline{K}_{pp}$	4.248

The above results indicate that the disharmony among three VSCUs causes a significant increase in power oscillation peak and average power from $VSCU_1$ on line 1-0. Moreover, Fig. 7(d) reveals that the average power is negative for a longer time during the disharmony period. The average power of line 1-0 is transmitted in the positive direction under HOC. During the disharmony period, however, the delivery direction of the average power of line 1-0 is positive for a portion of the time and negative for the remainder. This demonstrates that the disharmony not only leads to the peak amplification impact of oscillation in particular time intervals, threatening power grid stability, but also threatens the power balance between two equivalent networks at two terminals of line owing to inverse power transmission.

Section VI-B demonstrates that the load power flow including voltage, current, power peak, and average value of the non-active bus, and the line power flow including current, power peak, and average value, exhibit periodic variations instead of remaining steady and constant due to the disharmony among VSCUs in the LPG. In general, the disharmony period is significantly longer than the utility period of the AC grid (0.02 s), which can range from 10 s to 10^3 s or more, depending on the frequency difference between VSCUs. As a result, the period of disharmony oscillation is long.

4) Analysis of Effects of Synchronization and Harmonization Abilities on Proposed Indicators

The influence of the synchronization and harmonization abilities on oscillation will be further analyzed in this part. $f_{\oplus}$ or $T_{\oplus}$ reflects the harmonization ability. The synchronizing power coefficient reflects the synchronization ability. The synchronizing power coefficient is related to the initial phase difference between both sides of transmission line. Consequently, it is necessary to investigate the influence of $f_{\oplus}$ and initial phase difference on proposed indicators, including the swelling and sagging indicators and multiplication gains.

Figures 8 and 9 illustrate the variation of indicators. In Fig. 8(a), when $f_{\oplus}\in[0.001, 0.015]$Hz and $\varphi_{10}\in(0°, 15.06°]$, $\kappa_{swe-v}\in(100\%, 102.08\%)$, whose variation range is small, and the trend is similar to that of κ_{swe-c}. In Fig. 8(b) and (c), κ_{sag-v} and κ_{sag-p} do not monotonically increase or decrease. In Fig. 9, when φ_{10} increases and $f_{\oplus}$ remains constant, K_{cp}, K_{pp}, and $\overline{K}_{pp}$ decrease. By contrast, when $f_{\oplus}$ changes and φ_{10} remains certain, K_{cp}, K_{pp}, and $\overline{K}_{pp}$ change less.

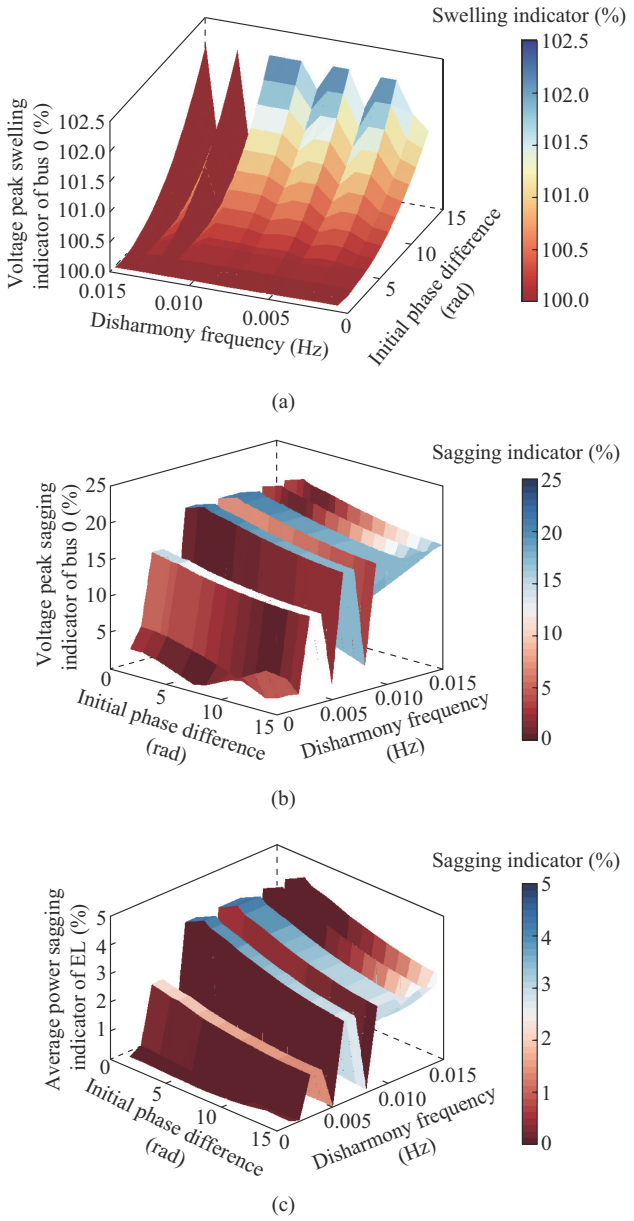

Fig. 8. Trend of swelling and sagging indicators with varying disharmony frequency and initial phase difference. (a) Voltage peak swelling indicator of bus 0. (b) Voltage peak sagging indicator of bus 0. (c) Average power sagging indicator of EL.

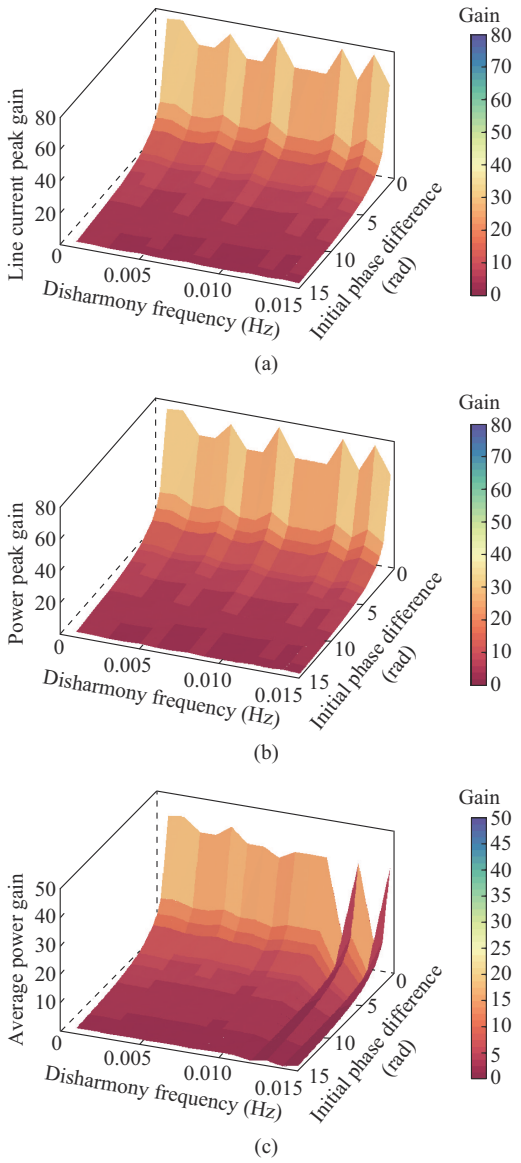

Fig. 9. Trend of oscillation peak gain with varying disharmony frequency and initial phase difference. (a) Line current peak gain. (b) Power peak gain. (c) Average power gain.

The following remarks can be obtained from Figs. 8 and 9. ① The characteristic indicators of EL at non-active bus are less sensitive to the changes in frequency but more sensitive to the changes in disharmony frequency and initial phase difference. ② The current and power multiplication gains of line connected to the VSCU are less sensitive to the changes in disharmony frequency and more sensitive to the changes in initial phase difference.

The changes in characteristic indicators and multiplication gains illustrate disharmony-induced qualitative changes, and the changes in the length of the disharmony period are more usually characterized as disharmony-induced quantitative changes. Although some of the parameters are less sensitive to the changes in disharmony period and initial phase difference, disharmony essentially leads to abnormal indicators. Whatever the degree of abnormality, it will have an impact on the power grid security and must thus be taken seriously.

C. Expanded Discussion on Multi-disharmony State Switching Scenario

If VSCUs lack frequency-harmonization control or have poor frequency-harmonization ability in a LPG or interconnected regional power grids, the power grid is likely to experience a continual disharmony oscillation from one disharmony state to the next. For multi-disharmony state switching scenario, let the Y-type three-terminal LPG in Fig. 2 operate under the disharmony state I at 0 s and switch to the disharmony states II and III at 250 s and 1350 s successively. The parameters of test system under switching scenario of 3-disharmony states are shown in Table VII, and other parameters are the same as in Section VI-A.

TABLE VII
PARAMETERS OF TEST SYSTEM UNDER SWITCHING SCENARIO OF 3-DISHARMONY STATES

Disharmony state	Output frequency of VSCU (Hz)			Parameters of load at bus 0		Disharmony period $T_{\oplus}$ (s)	Disharmony state duration (s)
	f_1	f_2	f_3	P_0 (MW)	$\cos\varphi_0$		
I	50.010	49.99	50.005	200	0.95	200	250
II	50.008	49.99	50.005	200	0.95	1000	1100
III	50.008	49.99	50.004	250	0.95	500	600

Figure 10 shows the average power of EL at bus 0, and average power of line 1-0 under the switching scenario of 3-disharmony states. Multi-disharmony state transformation causes prolonged disharmony oscillations.

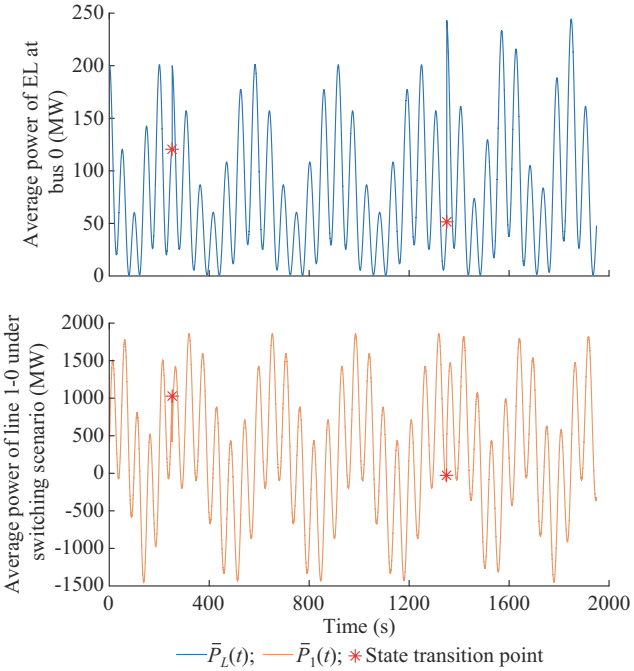

Fig. 10. Average power of EL at bus 0 and average power of line 1-0 under load switching scenario of 3-disharmony states.

In Table VII, the order of magnitude of any output frequency variation of VSCU between different disharmony

states is 10^{-3} Hz. The order of magnitude is likely to be lower than 10^{-3} Hz, while the frequency measurement accuracy and VSCU frequency output control accuracy are improved. Furthermore, the disharmony states usually do not switch at the integer-period point and there are disturbances in the power grid such as random noise and non-random active control. Consequently, the disharmony oscillations observed in the actual power grid are periodic or irregular oscillations, or the mixture of both with long duration.

VII. Conclusion

This paper analyzes the characteristics of power oscillation for the three-terminal power network with integration of three disharmonized VSCUs. The conclusions drawn from the analysis are given below.

1) Disharmony results in grid-side power oscillations. The disharmony period, which ranges from minutes to hours, is generally longer and much larger than the fundamental cycle.

2) The characteristic indicators indicate that disharmony results in a seriously lower load capacity and a significant amplification effect. The amplification effect is related to disharmony frequency and the initial phase difference. These indicators can provide information to identify whether the power grid is experiencing disharmony or will enter a disharmony state.

3) The investigation for switching among multi-disharmony states shows that considering the effects of disturbances such as random noise and active control in the power grid, the disharmony power oscillations in the actual power grid tend to manifest as periodic or irregular oscillations or the mixture of both with long duration.

4) In future research, we will design oscillation controllers based on frequency measurement information of each VSCU, monitoring information such as relevant characteristic indicators, or both types of information to address disharmony oscillations with a high proportion of VSCU integration.

Appendix A

The superposition theorem is applied to calculate $u_0(t)$, and the derivation process is as follows.

When the system frequency is f_1, the single-phase voltage phasor $\boldsymbol{U}_{0(1)}(\omega_1)$ of bus 0 is:

$$\begin{cases} \boldsymbol{U}_{0(1)}(\omega_1)=\dfrac{Z_\Sigma(\omega_1)\boldsymbol{U}_1(\omega_1)}{Z_1(\omega_1)+Z_\Sigma(\omega_1)}=k_{v1}(\omega_1)\mathrm{e}^{\mathrm{j}\beta_{v1}(\omega_1)}\boldsymbol{U}_1(\omega_1) \\ Z_\Sigma(\omega_1)=Z_2(\omega_1)//Z_3(\omega_1)//\dfrac{1}{\mathrm{j}\omega_1 C_{\mathrm{sum}}}//Z_{\mathrm{L}}(\omega_1) \end{cases} \tag{A1}$$

where $\boldsymbol{U}_1(\omega_1)$ is the single-phase voltage phasor of bus 1 when the system frequency is f_1; the symbol "//" denotes impedance parallel calculation; $k_{v1}(\omega_1)$ and $\beta_{v1}(\omega_1)$ are the impedance module and angle of $Z_\Sigma(\omega_1)/(Z_1(\omega_1)+Z_\Sigma(\omega_1))$, respectively, which are functions of ω_1; the impedance $Z_{\mathrm{L}}(\omega_1)$ of EL, each line impedance $Z_i(\omega_1)$, and total shunt capacitance C_{sum} at bus 0 are:

$$\begin{cases} Z_{\mathrm{L}}(\omega_1)=R_{\mathrm{L}}+\mathrm{j}\omega_1 L_{\mathrm{L}} \\ Z_i(\omega_1)=R_i+\mathrm{j}\omega_1 L_i \quad i=1,2,3 \end{cases} \tag{A2}$$

$$C_{\mathrm{sum}}=C_1+C_2+C_3 \tag{A3}$$

For the equivalent circuit with only one CVS at bus 1, single-phase instantaneous voltages $u_{0(1)}(t)$ of bus 0 can be derived by (A1) as:

$$u_{0(1)}(t)=H_1\sin(\omega_1 t+\alpha_{v1}) \tag{A4}$$

where the voltage peak H_1 and voltage initial phase α_{v1} can be obtained as:

$$\begin{cases} H_i=k_{vi}(\omega_i)U_{mi} \\ \alpha_{vi}=\varphi_i+\beta_{vi}(\omega_i) \end{cases} \quad i=1,2,3 \tag{A5}$$

Similarly, for the equivalent circuit with only one CVS at bus 2 or 3, single-phase instantaneous voltages $u_{0(2)}(t)$ or $u_{0(3)}(t)$ of bus 0 can be obtained. $u_0(t)$ of bus 0 can be expressed by:

$$u_0(t)=U_{m0}(t)\sin\psi_v(t) \tag{A6}$$

$U_{m0}(t)$ and $\psi_v(t)$ can be obtained as:

$$U_{m0}(t)=\left(\sum_{i=1}^{3}H_i^2+2H_1H_2\cos(\omega_{12}t+\alpha_{v1}-\alpha_{v2})+2H_1H_3\cos(\omega_{13}t+\alpha_{v1}-\alpha_{v3})+2H_2H_3\cos(\omega_{23}t+\alpha_{v2}-\alpha_{v3})\right)^{\frac{1}{2}} \tag{A7}$$

$$\psi_v(t)=\mathrm{mod}(\omega_3 t+\alpha_{v\oplus}(t),2\pi) \tag{A8}$$

Furthermore, initial phase $\alpha_{v\oplus}(t)$ of load voltage in the $\omega_\oplus$ reference frame and the difference ω_{ij} ($i=1,2$, $j=2,3$, $i<j$) between angular frequency of bus i and j are given as:

$$\alpha_{v\oplus}(t)=\mathrm{mod}(\mathrm{atan2}(H_1\cos(\omega_{13}t+\alpha_{v1})+H_2\cos(\omega_{23}t+\alpha_{v2})+H_3\cos\alpha_{v3},H_1\sin(\omega_{13}t+\alpha_{v1})+H_2\sin(\omega_{23}t+\alpha_{v2})+H_3\sin\alpha_{v3}),2\pi) \tag{A9}$$

$$\begin{cases} \omega_{12}=\omega_1-\omega_2 \\ \omega_{13}=\omega_1-\omega_3 \\ \omega_{23}=\omega_2-\omega_3 \end{cases} \tag{A10}$$

When $\omega_1\neq\omega_2\neq\omega_3$, $U_{m0}(t)$ is a periodic function, and its period $T_\oplus$ is:

$$T_\oplus=1/f_\varepsilon \tag{A11}$$

where f_ε is the fundamental element of the frequency. Meanwhile, the following condition must be met: integer outcomes f_1/f_ε, f_2/f_ε, and f_3/f_ε are coprime. The period $T_\oplus$ can reflect the severity of disharmony. Namely, the shorter $T_\oplus$ is, the more regularly high-risk disharmony phenomena such as peak amplification will occur.

Appendix B

When $\omega_1=\omega_2=\omega_3$, the load current peak $I_{\mathrm{Lm}}^{[\mathrm{har}]}$ and its initial phase $\alpha_{c\oplus}^{[\mathrm{har}]}$ under HOCs can be derived from (12) and (13) as:

$$I_{\mathrm{Lm}}^{[\mathrm{har}]}=\left(\sum_{i=1}^{3}J_i^2+2J_1J_2\cos(\alpha_{c1}-\alpha_{c2})+2J_1J_3\cos(\alpha_{c1}-\alpha_{c3})+2J_2J_3\cos(\alpha_{c2}-\alpha_{c3})\right)^{\frac{1}{2}} \tag{B1}$$

$$\alpha_{c\oplus}^{[har]} = \mathrm{mod}\left(\mathrm{atan2}\left(\sum_{i=1}^{3} J_i \cos\alpha_{ci}, \sum_{i=1}^{3} J_i \sin\alpha_{ci}\right), 2\pi\right) \quad \text{(B2)}$$

When $\omega_1 \neq \omega_2 \neq \omega_3$, let $\omega_\oplus$ be the angular frequency reference, and $\psi_c(t)$ is given in another form by:

$$\psi_c(t) = \mathrm{mod}(\omega_\oplus t + \alpha_{c\oplus}^{[dishar]}(t), 2\pi) \quad \text{(B3)}$$

$$\begin{aligned}\alpha_{c\oplus}^{[dishar]}(t) = \mathrm{mod}((\omega_3 - \omega_\oplus)t + \mathrm{atan2}(J_1\cos(\omega_{13}t + \alpha_{c1}) + \\ J_2\cos(\omega_{23}t + \alpha_{c2}) + J_3\cos\alpha_{c3}, J_1\sin(\omega_{13}t + \alpha_{c1}) + \\ \alpha_{c2}) + J_2\sin(\omega_{23}t + J_3\sin\alpha_{c3}), 2\pi)\end{aligned} \quad \text{(B4)}$$

where $\alpha_{c\oplus}^{[dishar]}(t)$ is the initial phase of load current under DOCs.

APPENDIX C

When $\omega_1 = \omega_2 = \omega_3$, the line current peak $I_{lm}^{[har]}$ and its initial phase $\gamma_\oplus^{[har]}$ under HOCs can derived from (27) and (28) as:

$$\begin{aligned}I_{lm}^{[har]} = \Bigg(\sum_{i=1}^{3} M_i^2 + 2M_1M_2\cos(\gamma_1 - \gamma_2) + 2M_1M_3\cos(\gamma_1 - \gamma_3) + \\ 2M_2M_3\cos(\gamma_2 - \gamma_3)\Bigg)^{\frac{1}{2}}\end{aligned} \quad \text{(C1)}$$

$$\gamma_\oplus^{[har]} = \mathrm{mod}\left(\mathrm{atan2}\left(\sum_{i=1}^{3} M_i\cos\gamma_i, \sum_{i=1}^{3} M_i\sin\gamma_i\right), 2\pi\right) \quad \text{(C2)}$$

When $\omega_1 \neq \omega_2 \neq \omega_3$, $\delta(t)$ is given in another form by:

$$\delta(t) = \mathrm{mod}(\omega_\oplus t + \gamma_\oplus^{[dishar]}(t), 2\pi) \quad \text{(C3)}$$

$$\begin{aligned}\gamma_\oplus^{[dishar]}(t) = \mathrm{mod}((\omega_3 - \omega_\oplus)t + \mathrm{atan2}(M_1\cos(\omega_{13}t + \gamma_1) + \\ M_2\cos(\omega_{23}t + \gamma_2) + M_3\cos\gamma_3, M_1\sin(\omega_{13}t + \gamma_1) + \\ M_2\sin(\omega_{23}t + \gamma_2) + M_3\sin\gamma_3), 2\pi)\end{aligned} \quad \text{(C4)}$$

REFERENCES

[1] J. Shair, H. Li, J. Hu *et al*., "Power system stability issues, classifications and research prospects in the context of high-penetration of renewables and power electronics," *Renewable & Sustainable Energy Reviews*, vol. 145, pp. 1-16, Jul. 2021.

[2] L. Chen, Y. Min, L. Hao *et al*., "Large-disturbance stability analysis of power systems with synchronous generator and converter-interfaced generation," *Journal of Modern Power Systems and Clean Energy*, vol. 12, no. 3, pp. 997-1002, Mar. 2024.

[3] Y. Meng, H. Wang, Z. Duan *et al.*, "Small-signal stability analysis and improvement with phase-shift phase-locked loop based on back electromotive force observer for VSC-HVDC in weak grids," *Journal of Modern Power Systems and Clean Energy*, vol. 11, no. 3, pp. 980-989, May 2023.

[4] L. G. Meegahapola, S. Bu, D. P. Wadduwage *et al*., "Review on oscillatory stability in power grids with renewable energy sources: monitoring, analysis, and control using synchrophasor technology," *IEEE Transactions on Industrial Electronics*, vol. 68, no. 1, pp. 519-531, Jan. 2021.

[5] N. Hatziargyriou, J. Milanovic, C. Rahmann *et al*., "Definition and classification of power system stability – revisited & extended," *IEEE Transactions on Power Systems*, vol. 36, no. 4, pp. 3271-3281, Jul. 2021.

[6] X. Wang, M. G. Taul, H. Wu *et al*., "Grid-synchronization stability of converter-based resources – an overview," *IEEE Open Journal of Industry Applications*, vol. 1, pp. 115-134, Sept. 2020.

[7] R. Pan, G. Tang, S. Liu *et al*., "Impedance analysis of grid forming control based modular multilevel converters," *Journal of Modern Power Systems and Clean Energy*, vol. 11, no. 3, pp. 967-979, May 2023.

[8] P. Kundur, J. Paserba, V. Ajjarapu *et al*., "Definition and classification of power system stability IEEE/CIGRE joint task force on stability terms and definitions," *IEEE Transactions on Power Systems*, vol. 19, no. 3, pp. 1387-1401, Aug. 2004.

[9] H. Gong, X. Wang, and L. Harnefors, "Rethinking current controller design for PLL-synchronized VSCs in weak grids," *IEEE Transactions on Power Electronics*, vol. 37, no. 2, pp. 1369-1381, Feb. 2022.

[10] X. Lin, R. Yu, J. Yu *et al*., "Constant-coupling-effect-based PLL for synchronization stability enhancement of grid-connected converter under weak grids," *IEEE Transactions on Industrial Electronics*, vol. 70, no. 11, pp. 11310-11323, Nov. 2023.

[11] C. Yang, L. Huang, H. Xin *et al*., "Placing grid-forming converters to enhance small signal stability of PLL-integrated power systems," *IEEE Transactions on Power Systems*, vol. 36, no. 4, pp. 3563-3573, Jul. 2021.

[12] L. Huang, H. Xin, Z. Li *et al*., "Grid-synchronization stability analysis and loop shaping for PLL-based power converters with different reactive power control," *IEEE Transactions on Smart Grid*, vol. 11, no. 1, pp. 501-516, Jan. 2020.

[13] M. G. Taul, X. Wang, P. Davari *et al*., "An overview of assessment methods for synchronization stability of grid-connected converters under severe symmetrical grid faults," *IEEE Transactions on Power Electronics*, vol. 34, no. 10, pp. 9655-9670, Oct. 2019.

[14] Y. Li, X. Wang, J. Guo *et al*., "PLL Synchronization stability analysis of MMC-connected wind farms under high-impedance AC faults," *IEEE Transactions on Power Systems*, vol. 36, no. 3, pp. 2251-2261, May 2021.

[15] Q. Hu, L. Fu, F. Ma *et al*., "Analogized synchronous-generator model of PLL-based VSC and transient synchronizing stability of converter dominated power system," *IEEE Transactions on Sustainable Energy*, vol. 12, no. 2, pp. 1174-1185, Apr. 2021.

[16] J. Chen, M. Liu, H. Geng *et al*., "Impact of PLL frequency limiter on synchronization stability of grid feeding converter," *IEEE Transactions on Power Systems*, vol. 37, no. 3, pp. 2487-2490, May 2022.

[17] T. Wu, Q. Jiang, M. Huang *et al*., "Synchronization stability of grid-following converters governed by saturation nonlinearities," *IEEE Transactions on Power Systems*, vol. 37, no. 5, pp. 4102-4105, Sept. 2022.

[18] Y. Qi, H. Deng, J. Fang *et al*., "Synchronization stability analysis of grid-forming inverter: a black box methodology," *IEEE Transactions on Industrial Electronics*, vol. 69, no. 12, pp. 13069-13078, Dec. 2022.

[19] J. Yu, Y. Qi, H. Deng *et al*., "Evaluating small-signal synchronization stability of grid-forming converter: a geometrical approach," *IEEE Transactions on Industrial Electronics*, vol. 69, no. 9, pp. 9087-9098, Sept. 2022.

[20] Z. Yang, M. Zhan, D. Liu *et al*., "Small-signal synchronous stability of a new-generation power system with 100% renewable energy," *IEEE Transactions on Power Systems*, vol. 38, no. 5, pp. 4269-4280, Sept. 2023.

[21] R. Rosso, X. Wang, M. Liserre *et al*., "Grid-forming converters: control approaches, grid-synchronization, and future trends – a review," *IEEE Open Journal of Industry Applications*, vol. 2, pp. 93-109, Apr. 2021.

[22] H. Wu and X. Wang, "A mode-adaptive power-angle control method for transient stability enhancement of virtual synchronous generators," *IEEE Journal of Emerging and Selected Topics in Power Electronics*, vol. 8, no. 2, pp. 1034-1049, Jun. 2020.

[23] X. Xiong, C. Wu, B. Hu *et al*., "Transient damping method for improving the synchronization stability of virtual synchronous generators," *IEEE Transactions on Power Electronics*, vol. 36, no. 7, pp. 7820-7831, Jul. 2021.

[24] D. Pan, X. Wang, F. Liu *et al*., "Transient stability of voltage-source converters with grid-forming control: a design-oriented study," *IEEE Journal of Emerging and Selected Topics in Power Electronics*, vol. 8, no. 2, pp. 1019-1033, Jun. 2020.

[25] T. Liu and X. Wang, "Transient stability of single-loop voltage-magnitude controlled grid-forming converters," *IEEE Transactions on Power Electronics*, vol. 36, no. 6, pp. 6158-6162, Jun. 2021.

[26] C. A. Savalov, *Operation Mode of the Unified Power System*. Beijing: Hydropower Press, 1988, pp. 94-119.

[27] Q. Yu and Y. Tang. (2023, Sept.). Mechanism analysis of power oscillation caused by disharmony of voltage source controlled-units at both sides of transmission line. [Online]. Available: http://kns.cnki.net/kcms/detail/11.2107.TM.20230918.1455.006.html

[28] R. Rosso, X. Wang, M. Liserre *et al*., "Grid-forming converters: control approaches, grid-synchronization, and future trends – a review," *IEEE Open Journal of Industry Applications*, vol. 2, pp. 93-109, Apr. 2021.

Qiyi Yu received the B.S. degree in electrical engineering from Shandong University, Jinan, China, in 2017, and the M.S. degree from Nanjing Nor-

mal University, Nanjing, China, in 2020. She is currently pursuing the Ph.D. degree at the School of Electrical Engineering, Southeast University, Nanjing, China. Her main research interest includes wide-frequency oscillation.

Yi Tang received the B.E., M.E., and Ph.D. degrees from Harbin Institute of Technology, Harbin, China, in 2000, 2002, and 2006, respectively. He is currently a Professor at the School of Electrical Engineering, Southeast University, Nanjing, China. His research interests include smart grid, power system security, power system stability analysis, renewable energy system, and cyber-physical system.